

**Citation**

Hernandez, F. and Zhang, X. and Hao, H. 2020. On the effectiveness of ventilation to mitigate the damage of spherical membrane vessels subjected to internal detonations. *International Journal of Protective Structures*. 11 (3): pp. 319-339. <http://doi.org/10.1177/2041419619900517>

# On the effectiveness of ventilation to mitigate the damage of spherical membrane vessels subjected to internal detonations

Francisco Hernandez<sup>1</sup>, Xihong Zhang<sup>2</sup>, and Hong Hao<sup>3</sup>

<sup>1</sup>Professor, School of Civil Engineering, University of Chile, Chile, [fhernandezp@ing.uchile.cl](mailto:fhernandezp@ing.uchile.cl)

<sup>2</sup>Senior Research Fellow, Department of Civil Engineering, Curtin University, Australia, [xihong.zhang@curtin.edu.au](mailto:xihong.zhang@curtin.edu.au)

<sup>3</sup>Professor, Department of Civil Engineering, Curtin University, Australia, [hong.hao@curtin.edu.au](mailto:hong.hao@curtin.edu.au)

**Abstract**

This paper conducts a comparative study on the effectiveness of ventilation to mitigate blasting effects on spherical chambers subjected to internal detonations of High Explosives (HE) through Finite Element Analysis (FEA) using the software package AUTODYN. Numerical simulations show that ventilation is ineffective in mitigating the damage of spherical chambers subjected to internal HE explosions because the chamber response is mainly described by high-frequency membrane modes. Openings do not reduce the chamber response despite they can reduce the blast overpressure after the chamber reaches its peak response. Worse still, openings lead to stress concentration, which weakens the structure. Therefore, small openings may reduce the capacity of the chamber to resist internal explosions. In addition, because large shock waves impose the chamber to respond to a reverberation frequency associated with the re-reflected shock wave pulses, secondary re-reflected shock waves (SW) can govern the chamber response, and plastic/elastic resonance can occur to the chamber. Simulations show that the time lag between the first and the second shock wave ranges from 3 to 7 times the arrival time of the first shock wave, implying that the current simplified design approach should be revised. The response of chambers subjected to eccentric detonations is also studied. Results show that due to asymmetric explosions, other membrane modes may govern the chamber response and causes localized damage, implying that ventilation is also ineffective to mitigate the damage of spherical chambers subjected to eccentric detonations.

**Keywords:** Confined explosions; AUTODYN; gas pressure component; afterburning; plastic resonance; quasi-static temperature

**1 Introduction**

Membrane chambers are curved vessels that display low bending stresses in comparison to membrane stresses when they are subjected to internal or external pressures. If the wall thickness of the chamber is smaller than 10 times the mean radius, the membrane stresses become dominant, and bending stresses can be virtually ignored. When the chamber walls offer resistance to bending, flexural bending stresses occur in addition to membrane stresses. For example, flat surfaces or shallow conical heads are susceptible to significant bending stresses that are commonly concentrated around their boundaries. In other words, flexural walls are inefficient geometries because stresses are concentrated in small portions reducing significantly the internal energy that the chamber is able to absorb; in contrast, membrane vessels show an almost uniform stress distribution that involves the response of the entire chamber. Therefore, the preferred shapes that are employed for the

2

1 construction and design of pressure vessels are spheres, cylinders, cones, ellipsoids, tori,  
2 or a combination of these geometries.

3 The membrane response of a pressure vessel is commonly associated with a high  
4 stiffness that results in high natural frequencies. For example, the natural frequency  
5 associated with the Radial Breathing Mode (RBM) of steel monobloc spherical chambers,  
6  $f_n = \sqrt{E/2 \cdot \pi^2 \cdot \rho(1 - \nu) \cdot a^2}$  (Baker and Allen, 1958), ranges respectively from 0.5kHz  
7 to 3.0kHz for  $a=3000\text{mm}$  and  $a=500\text{mm}$ , where  $a$  = the mean chamber radius in mm,  
8  $\rho = 7800\text{kg/m}^3$  is the material density,  $\nu = 0.28$  is the Poisson's ratio,  $E = 217\text{GPa}$  is  
9 the material Young's modulus. These high natural frequencies are in the same order of  
10 magnitude of the reverberation frequency associated with secondary re-reflected shock  
11 waves (SWs), which are generated when an internal detonation of a High Explosive (HE)  
12 occurs inside a fully confined blast chamber. Therefore, spherical chambers may  
13 experience resonant responses due to multiple re-reflected shock waves (Buzukov, 1980;  
14 Hernandez, 2016; Hernandez et al., 2018; Zhdan, 1981).

15 Simplified analysis using the SDOF (Single-Degree of Freedom) method is  
16 commonly employed in design practice to analyze the blast response of spherical blast  
17 chambers. The SDOF approach assumed perfect spherical symmetry, and the system is  
18 subjected to a concentric spherical HE detonation; as a result, the radial response of the  
19 chambers is exclusively described by the radial breathing mode. It also assumes that the  
20 pressure components (first shock wave, re-reflected shock waves, and the gas pressure)  
21 can be modeled by a transient uniform radial pressure, which acts synchronically on the  
22 entire chamber wall. The solution of the SDOF system considering a perfect elastic-  
23 plastic response was analyzed by Hernandez et al. (2018), concluding that all pressure  
24 components contribute significantly to the chamber response. The secondary re-reflected  
25 shock waves can increase the peak response of spherical chambers up to 85% when elastic  
26 or plastic resonance occurs. In fact, chamber resonance was observed when re-reflected  
27 secondary shock waves coincide with a positive radial velocity of the chamber wall  
28 (Hernandez et al., 2018), which increases the work that is done by blast pressure and the  
29 internal energy absorbed by the chamber. The gas pressure component can also increase  
30 the chamber response, particularly when ductile chambers are analyzed. Previous studies  
31 found the gas pressure component could increase the ductility ratio up to 40% (when the  
32 chamber shows a ductility ratio of 5 associated with the first shock wave only) (Hernandez  
33 et al., 2018). Thus, it is inaccurate to assume that the first shock wave plays a dominant  
34 role and ignores the effect of other pressure components such as simplified approaches  
35 suggest (Baker and Allen, 1958; Dong et al., 2012). It was also demonstrated by  
36 Hernandez et al. (2018) that because the gas pressure is not released quick enough,  
37 spherical chambers can rapidly reach the peak response. As a result, the gas pressure can  
38 not be significantly relieved by a relatively small vent on the chamber (10-20% of the  
39 total chamber surface area), implying that small ventilation could be ineffective in  
40 mitigating the damage of spherical chambers. Nevertheless, ventilation can be useful to  
41 reduce the quasi-static high temperature associated with the gas that remains inside the  
42 chamber after the dynamic response phase is reached in a fully confined spherical  
43 chamber subjected to an internal HE detonation.

44 The elastic resonance of spherical chambers subjected to concentric HE detonations  
45 was first observed by Zhdan (1981). Zhdan described and solved a one-dimensional gas-  
46 dynamic system of equations to determine the blast load that acts on rigid walls of  
47 spherical chambers. It was found that the period of intrinsic oscillation of the pressure  
48 can coincide or be a multiple of the natural chamber period; therefore "the effect of  
49 macro-pulsations at the wall has been derived; and the possibility of resonance of the  
50 chamber has been established and the corresponding condition noted" (Zhdan, 1981).

Similarly, Buzukov (1980) investigated experimentally the responses of cylindrical chambers subjected to the detonation of DSh-A explosive in strips. It was found that the secondary deformation of the chamber is due to resonance arising from the combination of the longitudinal and radial vibration of several harmonics. Results also indicated that the leading cause of the increasing strain lies in the repeatedly reflected shock waves because, under certain conditions, the interval between the pulses loads is close to the period of oscillation of the body. Buzukov (1980) reported 10 relatively strong reflected shock waves were observed during his experimental study. The author also observed that the arrival time related to the second and subsequent reflected shock waves were not proportional to the arrival time of the first shock wave. As a consequence, the simplified approach proposed by Anderson and Baker (1983) to estimate the effect of the shock wave reflection should be further reviewed when the resonance phenomena need to be accounted for.

Comprehensive numerical modeling has also been conducted to study the blast response of blast chambers. FEA and CFD (Coupled Fluid Dynamics) methods, with coupled or uncoupled Lagrange-Euler algorithms, have been developed by different researchers (Dong et al., 2012; Trabia et al., 2008), which enable accurate modeling of the interactions between gaseous explosive products, i.e., air, gases, fluids, and structural elements, which can also be used to model more complex but realistic phenomena such as the presence of nozzles, complex geometries, effects of obstructions, different explosive shapes, diverse explosive materials, changes of ignition points (e.g., eccentricities), strain growth phenomena, multiple initial conditions (e.g., pressure, temperature, medium of propagation), nonlinear structural materials, the effect of three-dimensional membrane and bending modes, different pressure vessel technologies and other kinds of singularities that simplified method cannot take into account. FEA can also be used to perform parametric simulations to evaluate the consequences of these variables and to verify different design scenarios. Till now, there is no study yet using a detailed numerical model to investigate the effectiveness of opening for spherical chambers under internal blast loading.

In this study, a three-dimensional (3D) model of blast chambers with and without ventilation opening is carried out. The chamber model is coupled with an air blast domain. Comparisons are made between the numerical results from the 3D model and the simplified SDOF model as well as a 1D numerical model. The accuracy of these methods in predicting blast overpressures for both concentric and eccentric detonations are compared. The responses of the spherical chambers predicted using these methods are also evaluated.

## 2 Spherical Chambers subjected to concentric TNT detonations

Numerical simulations are carried out using the software package ANSYS AUTODYN v14.0. A detailed numerical model of the spherical chamber subjected to concentric TNT detonation is generated and simulated. As shown in Figure 1, a monobloc spherical chamber with a mean radius  $a=1500\text{mm}$  is generated. Two wall thicknesses are considered, which are related to two different performance levels: ductility ratios equal to 1.0 and 5.0. The chambers with and without openings are both modeled to evaluate the effect of ventilation. Chamber with opening, i.e., partially confined chambers are modeled with 8 circular openings (273.6mm radius) that provides an equivalent vent area  $A_v/A_{chamber} = 6.72\%$  (where  $A_v$  is the total vent area,  $A_{chamber}$  is the total surface). The value corresponds to the maximum vent area that can be employed by using Anderson's approach (1983) to estimate the gas pressure component for partially confined chambers subjected to internal TNT detonations. 7kg, 15kg, 30kg, and 120kg of spherical TNT

4

charges are modeled in this study. Considering symmetry, only one-eighth of the spherical chamber is modeled to save computational time. Fully coupled Euler/Lagrange interaction is employed. Remapping techniques were used, i.e., an initial 1D Euler multi-material simulation with a finer mesh (0.2mm size) was employed to simulate the initial radial propagation before that the first shock wave reaches the spherical chamber wall. A cubical multi-material 3D-Euler element of 13.3mm edge sizes are employed. This implies that a total of 1,728,000 elements are used to model air and TNT, by using a Euler domain size of 1.6m x1.6m x1.6m=4.096m<sup>3</sup> (different meshing sizes were considered to verify mesh effects, which are later discussed in section 2.4). The shell thickness was twice of the Euler element size (i.e., 27mm) in order to ensure the proper Euler/Lagrange interaction. 5 layers of shell elements were used to model the blast chamber (1300 elements).

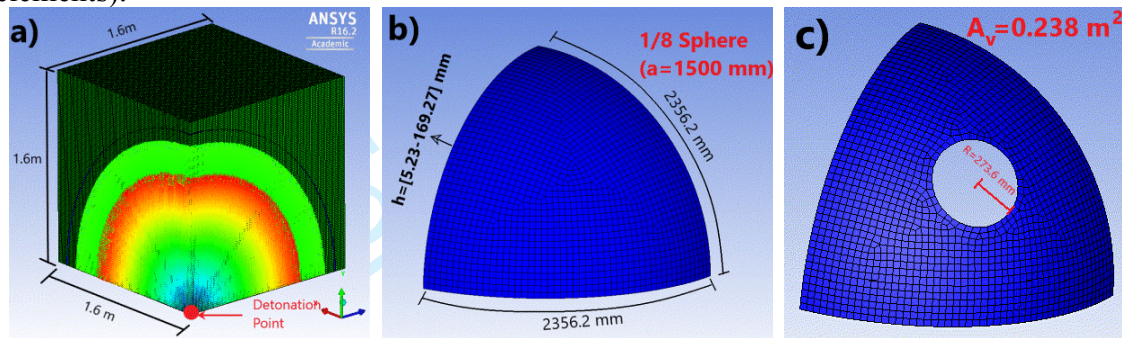


Figure 1: AUTODYN 3D model of fully confined (FC) and partially confined (PC) chambers: a) Euler mesh and initial remapped shock wave, b) FC Lagrange shell mesh, c) PC Lagrange shell mesh.

## 2.2 Material models

The JWL EOS with the AUTODYN's default parameters is employed to model TNT gas products

$$P_{TNT}^{JWL}(v, E^{TNT}) = A \cdot e^{-R_1 \cdot v} \cdot \left[ 1 - \frac{\omega}{v \cdot R_1} \right] + B \cdot e^{-R_2 \cdot v} \cdot \left[ 1 - \frac{\omega}{v \cdot R_2} \right] + \frac{\omega \cdot \rho_0^{TNT} \cdot E^{TNT}}{v} \quad (1)$$

where  $v = \rho_0^{TNT} / \rho^{TNT}$ ,  $A = 3.7377 \cdot 10^8 \text{ kPa}$ ,  $B = 3.7471 \cdot 10^6 \text{ kPa}$ ,  $R_1 = 4.15$ ,  $R_2 = 0.9$ ,  $\omega = 0.35$ .

Similarly, the ideal gas EOS is used for air (with  $\gamma_{air} = 1.4$ )

$$P_{air}^{ideal}(\rho_{air}, E_{air}) = \rho_{air} \cdot (\gamma_{air} - 1) \cdot E_{air} \quad (2)$$

The initial internal energy and density are selected, assuming that air is at standard temperature and pressure (*stp*), i.e., 298K and 1atm. Therefore,  $E_0^{air} = 2.068 \times 10^5 \text{ J/kg}$  is the initial specific internal energy of air,  $\rho_0^{air} = 0.001225 \text{ g/cm}^3$  is the initial air density. Similarly, the initial TNT density is  $\rho_0^{TNT} = 1.63 \text{ g/cm}^3$  and  $E_0^{TNT} = 36.8098 \times 10^6 \text{ J/kg}$ . The same additional afterburning energy is used for fully confined and partially confined explosions.

A bilinear isotropic hardening material (perfect elastic-plastic material) for steel chamber with properties associated with steel BHW35 with density  $\rho_s = 7800 \text{ kg/m}^3$ , Bulk modulus  $K = 1.644 \cdot 10^8 \text{ kPa}$ , shear modulus  $G = 84.76 \text{ GPa}$ , Young's modulus  $E = 2.17 \times 10^5 \text{ MPa}$ , and a yielding strength  $\sigma_y = 3.9 \times 10^5 \text{ kPa}$ . Strain rate effect, viscous elastic damping, and thermal effects are ignored.

Table 1 summarizes parameters used for simulations, where,  $W$  is the concentric charge weight (ignited at the center of the chamber and has a spherical shape),  $h$  is the



thickness of the spherical blast chamber (for ductility ratios  $\mu=1$  and  $\mu=5$  following Case 1S in Hernandez et al. (2018)),  $R$  is the initial TNT charge radius,  $\bar{r} = r/R$  is the relative distance (Shin et al., 2014), (where  $r = a - h_{\mu=5}/2$  is the distance from the TNT charge to the chamber wall),  $V_{\text{vessel}}$  is the vessel's volume,  $\Delta E_{\text{ad}}$  is the additional afterburning energy,  $P_{\text{UFC}}$  is the absolute quasi-static (QS) gas pressure according to UFC (UFC 3-340-02, 2008),  $t_a$  is the arrival time of the first shock wave,  $t_r = i_r \cdot 2/p_r$  is the duration of the equivalent triangular first shock wave pulse that is obtained from the UFC (UFC 3-340-02, 2008), based on the reflected impulse ( $i_r$ ) and the reflected pressure ( $p_r$ ).

Table 1: Parameters used in the simulation ( $a=1500\text{mm}$ )

TNT charge (W)	7 kg	15 kg	30 kg	120 kg
Thickness ( $h_{\mu=5}$ ) $\mu=5$	5.23 mm	9.62 mm	16.84 mm	54.93 mm
Thickness ( $h_{\mu=1}$ ) $\mu=1$	15.58 mm	28.84 mm	50.84 mm	169.27 mm
$R$	100.8 mm	130.0 mm	163.8 mm	260.0 mm
$\bar{r}$	14.85	11.50	9.11	5.66
$\bar{r} \cdot R / 82$	18.26 mm	18.23 mm	18.19 mm	17.96 mm
$\bar{r} \cdot R / 336$	-	-	4.44 mm	4.38 mm
$W/V_{\text{vessel}}$	0.498 kg/m <sup>3</sup>	1.071 kg/m <sup>3</sup>	2.158 kg/m <sup>3</sup>	8.972 kg/m <sup>3</sup>
$\Delta E_{\text{ad}}$	4085 kJ/kg	1407 kJ/kg	744.3 kJ/kg	0 kJ/kg
$P_{\text{UFC}}$	1570 kPa	2165 kPa	3544 kPa	11337 kPa
$t_a$	0.65 ms	0.53 ms	0.44 ms	0.34 ms
$5x(t_a + t_r)$	3.46 ms	2.92 ms	2.50 ms	2.08 ms

### 2.3 Additional afterburning energy and Ventilation

The additional afterburning energy ( $\Delta E_{\text{ad}}$ ), as listed in Table 1, is selected to ensure the QS gas pressure agrees with the QS gas pressure suggested by the UFC chart (UFC 3-340-02, 2008). It is assumed that the additional afterburning energy starts to be released after the first SW arrives at the chamber wall ( $t_a$ , Table 1). It is also assumed that  $\Delta E_{\text{ad}}$  is fully released after the third SW finishes impinging the chamber walls ( $5x(t_a + t_r)$ , Table 1), which agrees with the gas pressure growing rate observed by Baker from tests of chambers subjected to concentric detonations. It is also worth noting that CFD software packages, such as AUTODYN, are able to model the fluid dynamic process associated with the discharge of gases that occurs throughout openings. For example, Edri et al. (2012) used AUTODYN to model the venting process throughout a small circular opening on a cubical chamber. The pressure time-history obtained using AUTODYN was in good agreement with experimental data.

### 2.4 Mesh size effect

Shin et al. (2014) performed a mesh size sensitivity study to establish the optimum mesh size for 1D analysis using AUTODYN. It was concluded that converged solutions could be achieved for mesh sizes smaller than  $r/336$  if  $\bar{r} < 4.5$  (near field) or  $r/82$  when  $\bar{r} > 11$  (far-field). If the same level of convergence for 3D analyses is assumed, it is reasonable to assume that a mesh size of 13.3mm is suitable for  $W = 7\text{kg}$ , 15kg, and 30kg TNT explosion cases, but it may be not enough for  $W = 120\text{kg}$  (where 4.4mm mesh size

6

is required, implying 48 millions of Euler elements). In this study, another 1D model with mesh sizes of 0.75mm (chamber assumed to be perfectly rigid), together with the 3D model mentioned above were generated for the fully confined spherical chamber subjected to a concentric TNT detonation ( $W = 7\text{kg}$ ). Both models use the same additional afterburning energy detailed in Table 1. Figure 2 compares the overpressure results from the two numerical models with that from UFC prediction. It can be found that the 1D model showed a more significant energy error during its numerical solution (equal to 15%).

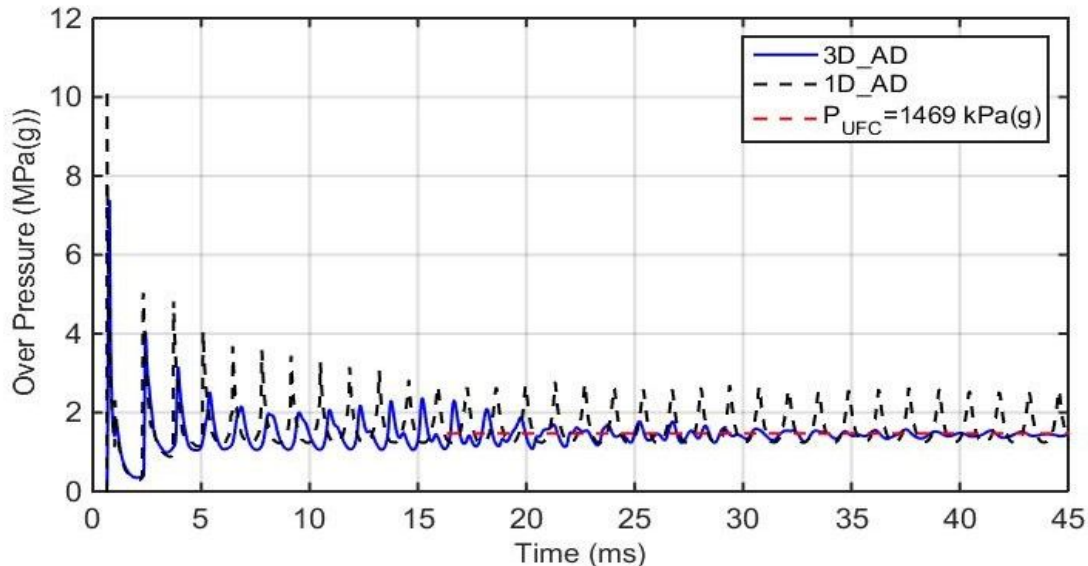


Figure 2. Overpressure time history obtained with the 3D and 1D models ( $a=1500\text{mm}$ ,  $W=7\text{kg}$ )

Figure 3a compares the pressure time-histories during the first 20ms obtained from 1D and 3D analyses (1D\_AD and 3D\_AD, respectively) as well as the prediction using the simplified SDOF approach (Hernandez, 2016). Very similar reflected pressures associated with the 1st SW ( $p_r$ ) can be found for the prediction of SDOF model (10.19MPa, obtained from the UFC chart) and the 1D analysis (10.21MPa); about 27.6% smaller reflected pressure ( $p_r = 7.38\text{MPa}$ ) is found on the 3D analysis. A small second shock wave is observed behind the shock front owing to the expansion of HE products (a reverberating shock wave) (Buzukov, 1980; Zhdan, 1981), which is not considered by the simplified SDOF approach). Also, the 3D model shows more than 10 significant shock waves, and the 1D analysis shows 33 significant shock waves during the first 45ms (after ignition) with limited attenuation. The difference is because the 3D model takes into account the fluid/structure interaction, the energy absorbed by the chamber, the imperfect asymmetrical behavior, and energy errors observed during the solution of the 1D FEA.

Table 2 shows the peak reflected pressures, arrival times, and reflected impulses associated with the first 10 shock waves obtained from the 1D analysis, the 3D analysis, and the simplified SDOF model. It can be observed that the peak reflected pressures predicted by the 3D model are 35% lower than that from the 1D analysis. The arrival times obtained from the 1D and 3D analyses are slightly different during the initial part of the curve, but the cumulative difference becomes significant after the 4th pulse. And the arrival times associated with the secondary re-reflected pulses calculated with the simplified approach are smaller than those obtained from numerical simulations. Overall, the 1D model shows slightly shorter arrival times than the 3D model. The reflected impulses (obtained between each pressure local minimum) do not show a significant difference between the three models. Nevertheless, similar QS gas pressures are predicted

7

1 by both the 1D and 3D models, which also agree well with the UFC prediction (1469kPa),  
 2 indicating the afterburning energy value was appropriate.

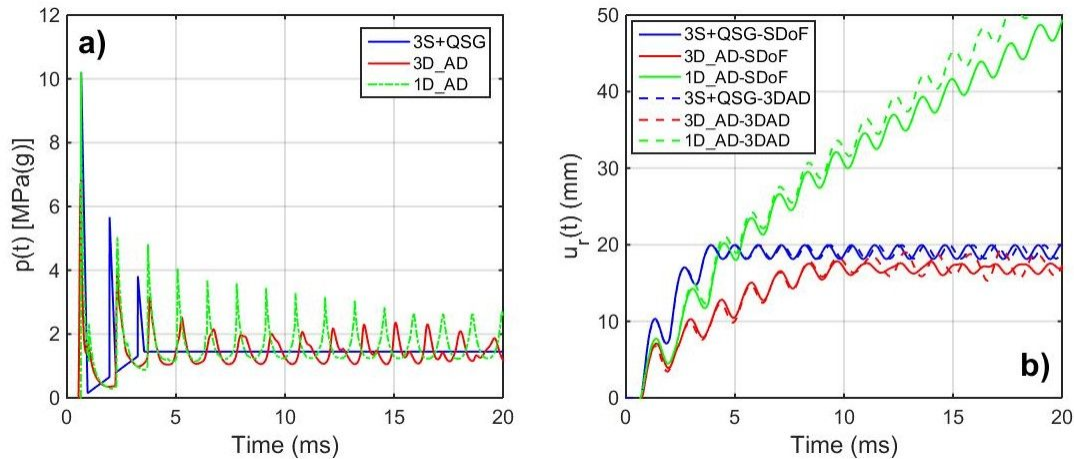


Figure 3. a) Overpressure time-history from SDOF model, 3D model, and 1D model; b) Radial response calculated with the equivalent SDOF system assuming coupled or uncoupled 3D analysis

Table 2: Peak reflected pressure ( $p_r$ ), arrival times ( $t_a$ ) and impulses ( $i_r$ ) related to the first 10 shock waves (SW) for 1D and 3D simulations and the simplified approach

SW No.	1D model (1D_AD)			3D model (3D_AD)			Simplified SDOF (Case 3S+QSG)		
	$p_r$ (MPa)	$t_a$ (ms)	$i_r$ (MPa ms)	$p_r$ (MPa)	$t_a$ (ms)	$i_r$ (MPa ms)	$p_r$ (MPa)	$t_a$ (ms)	$i_r$ (MPa ms)
1	10.21	0.64	2.04	7.58	0.64	2.01	10.19	0.65	1.92
2	2.31	1.01	-	1.69	0.97	-	-	-	-
3	5.02	2.31	2.26	4.05	2.30	1.84	5.67	1.95	2.00
4	4.82	3.71	2.22	3.16	3.81	2.07	3.82	3.25	2.22
5	4.07	5.07	1.74	2.52	5.26	1.93	-	(5.26)	2.08
6	3.68	6.44	2.17	2.15	6.72	2.11	-	(6.72)	2.11
7	3.58	7.78	2.07	1.84	7.99	2.13	-	(7.99)	2.15
8	3.44	9.13	2.18	2.00	9.39	2.06	-	(9.39)	2.06
9	3.27	10.49	2.13	2.06	10.80	2.06	-	(10.8)	2.06
10	3.15	11.84	2.22	2.17	12.21	2.12	-	(12.2)	2.13
$\frac{1}{t_a} = 714.6\text{Hz}$ $\sum = 19.0$ $\frac{1}{t_a} = 691.6\text{Hz}$ $\sum = 18.3$ $\frac{1}{t_a} = 769.2\text{Hz}$ $\sum = 18.7$									

\* $t_a$  is the average time difference between arrival times of subsequent shock waves.

### 3 2.5 Plastic resonance

4 Part of the energy, which is allocated in enclosed gases, is absorbed by the chamber  
 5 due to blast wave/structure interaction. The work that is done by the blast pressure ( $W_{gas}$   
 6 ( $t) = \int p(t) \cdot \dot{u}_r(t) dt$ , where  $\dot{u}_r$  is the chamber radial velocity) is highly related to the  
 7 internal energy that the chamber absorbs as a result of elastic or plastic deformation. This  
 8 process is not accounted for the 1D analyses since the chamber was assumed to be rigid

8

( $u_r = 0$ ). Therefore, uncoupled analyses cannot describe the attenuation of shock waves accurately. On the other hand, the 1D uncoupled analyses could be conservative for the design of blast chambers, because it does not take into account the attenuation of shock waves due to the energy absorption of the chamber.

Figure 3b shows the radial response of the chamber ( $u_r(t)$ ) calculated by using the pressure time-histories (Figure 3a). The radial response of the chamber is obtained using two procedures, i.e., the equivalent perfect elastic-plastic SDOF model (Hernandez, 2016) and by 3D Finite Element Analysis performed in the software package AUTODYN (3D\_AD). The SDOF solution is obtained by considering a perfect elastic-plastic response solved by using the Newmark's constant acceleration method (Chopra, 1995). Overall, the equation of motion that describe the radial response ( $u_r(t)$ ) of a spherical chamber subjected to a uniform pressure time-history ( $p(t)$ ) was described by Baker (1958) as follows,

$$\frac{\partial^2 u_r}{\partial t^2} + \omega_n^2 \cdot u_r = \frac{p(t)}{\rho \cdot h} \quad (3)$$

Where  $\rho =$  is the material density ( $kg/m^3$ ),  $\omega_n = \sqrt{2 \cdot E / (\rho \cdot (1 - \nu) \cdot a^2)}$  the natural angular frequency,  $P_y = 2 \cdot h \cdot \sigma_y / a$  is the yielding pressure,  $h$  is the chamber wall thickness (m),  $E =$  Young's modulus (Pa),  $\sigma_y =$  the yielding strength (Pa),  $\nu =$  the Poisson's ratio,  $a =$  the mean radius of the spherical chamber (m).

The radial responses 3S+QSG-3DAD and 1D\_AD-3DAD are obtained from uncoupled analyses, i.e., the pressure time-histories are uniformly applied to the chamber, while the radial response 3D\_AD-3DAD refers to a coupled analysis where the Euler/Lagrange interaction was directly accounted. From Figure 3b it can be found that the spherical chamber is highly susceptible to plastic resonance. In particular, the pressure time-history associated with the 1D analysis (1D-AD) generates several re-reflected pulses, which frequently coincide with positive radial velocities, and triggers amplification at short and long terms. The second SW associated with the pressure profile 3S+QSG coincides with higher radial velocities, causing a significant amplification on the response of the chamber. The smallest amplification caused by the second SW is observed for the pressure time-history 3D-AD. Because this SW coincides with smaller radial velocities, the pulses do not precisely resonant with the RBM. The occurrence of resonance depends on the arrival times associated with the re-reflected SW pulses. Therefore, a small difference in the arrival time can imply a significant difference in the amplification caused by pulses. In general, the arrival times of secondary SWs involve a certain degree of uncertainty. As previously mentioned, the way that the afterburning energy is released can change the arrival time, and the peak reflected pressure associated with each SWs (Hernandez et al., 2016).

The peak RBM response is described by the work that is done by the blast pressure, i.e.,  $u_r^{\max} = f(W_{gas})$ . It can be observed that the pressure time-histories, which were obtained with the 1D model (1D\_AD), the 3D model (3D\_AD), and the SDOF model (3S+QSG), have similar reflected impulse values ( $i_r$ ) associated with each shock wave (Table 2). However, significant differences in the chamber responses are observed (Figure 3b) because shock waves arrive at slightly different times, and the shape of the SWs is not precisely the same (Figure 3a). It can also be found that the reflected impulses ( $i_r$ ) associated with secondary SWs (SW>3) (shown in Table 2) are mainly associated with



the gas pressure component, rather than the effect of re-reflected pulses. Therefore, the reflected impulses of Table 2 are not related to the resonant phenomenon. Based on the analysis of the work by blast pressure, it can be concluded that the work of blast pressure increases when the chamber velocity is positive, and it decreases when a negative radial velocity occurs, owing to that the overpressure is always positive for confined explosions.

The second effect generated by the gas pressure component refers to the quasi-static stress. The gas pressure component causes uniform tensile membrane stress, which can be obtained from the static part of the equation of motion and equal to  $\sigma^{gas}(t) = a \cdot p^{gas}(t)/(2 \cdot h)$  (normal stresses) for spherical chambers, owing to the high-natural frequency of the RBM. The membrane stress is a constant,  $\sigma^{QS} = a \cdot P_{QS}/(2 \cdot h)$ , when the QS pressure ( $P_{QS}$ ) is reached. Thus, the QS gas pressure increases the average stress of the chamber wall, increasing the chance of the chamber plastic deformation. Since  $\sigma^{gas}(t)$  is a quasi-static function, it can be included in the analysis as a yielding strength reduction, i.e.,  $\sigma_y^{eff}(t) = \sigma_y - \sigma^{gas}(t)$ . Therefore, the simplified plastic resonance approach suggested by Hernandez et al. (2018) can be improved by considering the equivalent yield strength.

Figure 4 shows that the plastic response of the chamber is mainly governed by the SWs frequency (714.6 Hz and 691.6 Hz, Table 2). This implies that the blast load enforces the structure to respond at the excitation frequency, which is lower than the natural frequency of the chamber (932.7 Hz) when plastic behavior is observed. It can be found that the response obtained from the SDOF analysis is similar to the curve simulated from the 3D model. Therefore, the chamber response is mainly described by the RBM. This can be further proved by the 3D analysis results that show an almost uniform plastic strain distribution and a uniform radial deformation during the simulation (as shown in Figure 10).

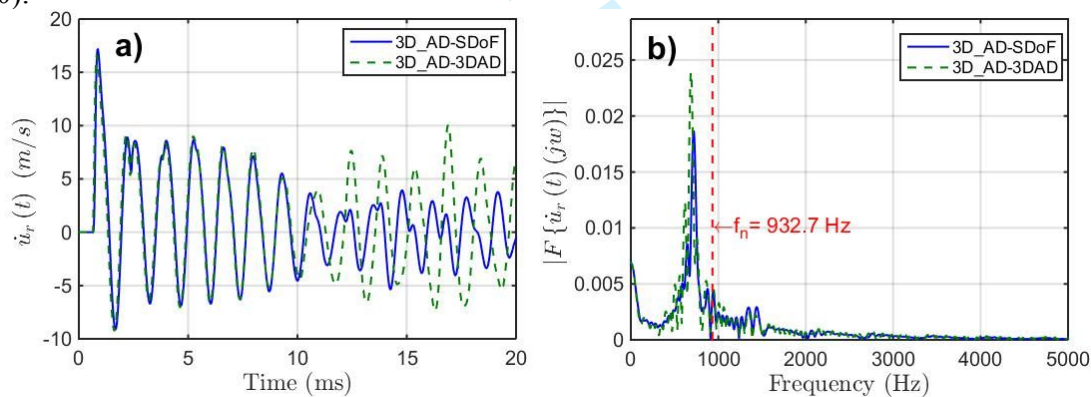


Figure 4 a) Radial velocity of the chamber and b) frequency spectrum obtained with the SDOF model and the coupled 3D model

From Figure 4a it can be observed that during the initial 10ms the radial velocity from the SDOF model and the 3D model match closely. When the 9<sup>th</sup> SW arrives at 10.8ms (Figure 3 and Table 2), the pulse coincides with a peak radial velocity, which generates an amplification for the 3D analysis. However, this SW does not exactly resonate with the SDOF solution because of a minor time lag between the 3D model and the SDOF analysis. A significant difference can be observed in the radial velocity between the 3D model and the SDOF model indicating that a small uncertainty in the response phase could lead to significant differences in the prediction of the response because the chamber resonance is highly susceptible to small changes in the arrival time of re-reflected shock waves. On the other hand, the chamber responses are governed by the RBM frequency (932.7Hz) when it behaves elastically. The chamber response is primarily governed by an impulsive component in agreement with the natural frequency of the system. Figure 5 shows the

10

1 elastic radial response (displacement and velocity) when an elastic chamber is used for  
 2 the SDOF analysis (i.e., large  $\sigma_y$ ). As can be found, the frequency spectrum is governed  
 3 by the elastic frequency of the chamber (932.7Hz), and a secondary peak is related to the  
 4 frequency related to SWs (691.7 Hz). It can also be observed from Figure 5 that the  
 5 chamber response is very similar when 1D\_AD or 3D\_AD pressure time-histories (Figure  
 6 3) are used. Resonance is not observed if the SW frequency does not coincide with the  
 7 natural frequency of the chamber. A beating effect can be observed related to the presence  
 8 of the natural RBM frequency and the re-reflected SWs frequency on the chamber  
 9 response but no amplification due to resonance, as observed above in Figure 3b.

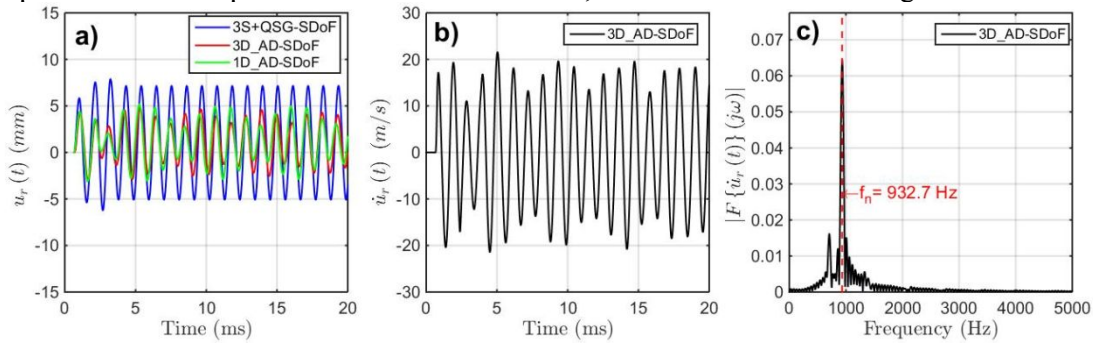


Figure 5. a) Radial response of the chamber, b) radial velocity and c) frequency spectrum obtained with the SDOF model for the elastic chamber ( $a=1500\text{mm}$ ,  $W=7\text{kg}$ )

10 Similarly, Figure 6 shows the chamber response and its frequency spectrum when the  
 11 structure is modified with a natural frequency equal to the re-reflected pulses (i.e.,  
 12 691.7Hz). It should be noted that without losing generality, this is artificially achieved by  
 13 modifying Young's elasticity modulus of steel to  $E = 119.35\text{GPa}$ . As shown, the  
 14 obtained chamber response by using the 3D\_AD and the 1D\_AD pressure time-histories  
 15 are quite similar. That is, both models show a significant amplification effect due to the  
 16 re-reflected shock waves for short and long terms. In other words, if the chamber  
 17 frequency is similar to the frequency of the pulses, small differences in shock wave  
 18 amplitudes have little influence on the chamber response.

19 Based on these results, it can be concluded that strong SWs induce force-vibration of  
 20 the chamber, and tend to lead to the plastic resonance of the chamber, i.e., peaks of SW  
 21 pulses tend to coincide with peak radial velocities. If blast waves are attenuated, the  
 22 response of the chamber tends to be governed by its natural frequency; therefore,  
 23 resonance occurs if the chamber's frequency is near to (or a multiple of) the frequency of  
 24 SW pulses only.

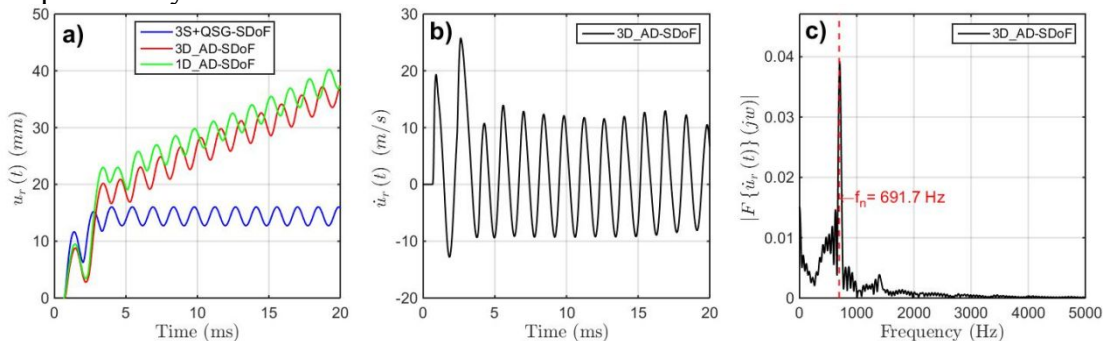


Figure 6. a) Radial response of the chamber, b) radial velocity and c) frequency spectrum obtained with the SDOF model when  $E = 1.1935 \times 10^5 \text{MPa}$

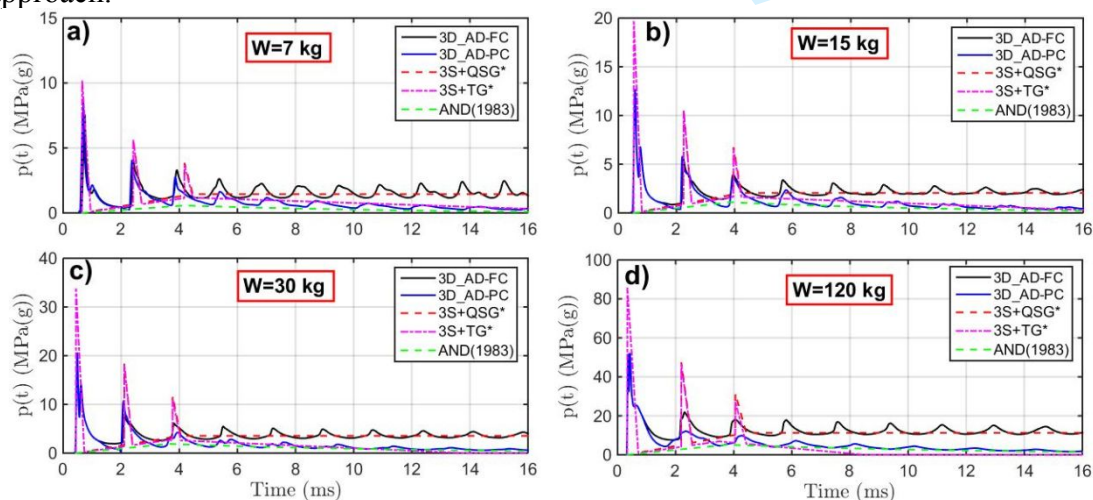
25 From Figure 4, it can also be observed that the peak chamber velocity tends to coincide  
 26 with the re-reflected shock wave peaks when pulses display a significant amplitude.

1 Instead, the peaks in the pressure time-histories do not coincide with radial peak velocities  
 2 when pulses are not strong enough. In other words, weak pulses are slowly uncoupled to  
 3 the chamber response, which prevents amplifications. As we can observe in Figure 3, the  
 4 plastic resonance for the 3D\_AD pressure is observed until 10ms, after which SW pulses  
 5 and the chamber response are slowly uncoupled, which leads to no plastic amplification.  
 6 The SDOF system is accurate to simulate the response of spherical chambers subjected to  
 7 concentric TNT detonations. This is because other asymmetrical and non-asymmetrical  
 8 modes, related to membrane and bending modes, have an insignificant contribution to the  
 9 chamber response. Therefore, the blast loading generates a uniform pressure that excites  
 10 only the RBM. The assumption that the initial three shock waves are the most important  
 11 and the subsequent SWs can be ignored may not necessarily be accurate for fully confined  
 12 spherical chambers, because subsequent re-reflected pulses can cause significant strain  
 13 growth due to a resonant response. The arrival times that are assumed by the simplified  
 14 pressure time-history (Case 3S+QSG,(Hernandez et al., 2018)) associated with secondary  
 15 re-reflected SWs are smaller than those predicted by the numerical models. Therefore,  
 16 the simplified approach that considers only the initial three SWs needs to be reviewed as  
 17 soon as the plastic resonance is highly susceptible to the effect of other secondary SWs.

## 18 2.6 Venting Effects

19 Ventilation in the chamber could have the following influence on the recorded  
 20 pressure-time history: i) reduces the gas pressure component; ii) reduces secondary re-  
 21 reflected SWs, and iii) the pressure profile is not uniform anymore. In the meanwhile, the  
 22 first SW is almost unaltered by small openings.

23 Figure 7 shows the overpressure time history obtained from coupled 3D model  
 24 (3D\_AD), for the fully confined (FC) case and the partially confined (PC) case when the  
 25 chamber is subjected to concentric detonations of TNT charges ( $W=7\text{kg}$ ,  $15\text{kg}$ ,  $30\text{kg}$ , and  
 26  $120\text{kg}$ ). The pressure time-histories from the 3D model are compared with those  
 27 estimated using the approaches suggested in the UFC (Case 3S+QSG\* and 3S+TG\*) by  
 28 considering three SWs. It is worth noting that the arrival time of the 2<sup>nd</sup> SW in the UFC  
 29 model is modified to coincide with the arrival time obtained from the 3D model for the  
 30 fully confined case (3D\_AD-FC). The 3rd SW is assumed to propagate at the same  
 31 average speed observed for the 2<sup>nd</sup> SW. Additionally, it has been included the gas pressure  
 32 component that was obtained for the partially confined case by using the Anderson (1983)  
 33 approach.



34 Figure 7 Overpressure time history obtained for the Fully Confined (FC) and Partially  
 35 Confined (PC) cases using the 3D model and the simplified SDOF model a)  $W=7\text{ kg}$ , b)  $15$

12

kg, c) 30 kg d) 120 kg

From Figure 7, it is observed that the QS gas pressure that was obtained for the fully confined case and the 3D model matches closely with that given by UFC (Table 1) if an appropriate additional afterburning energy value is used (Hernandez et al., 2016). Similarly, the gas pressure for the partially confined condition agrees well with the pressure component that is suggested by Anderson (1983) (which was obtained from adjustment of experimental data), and it is reasonably similar to the simplified triangular gas pressure component suggested by the UFC (which was also obtained from experimental data, but based on a simplified triangular curve). In other words, the pressure gas component obtained from the numerical solution is validated because it matches the experimental curves for the fully and partially confined cases. Therefore, it can be concluded that ventilation is correctly modeled when openings are incorporated in AUTODYN. Additionally, it can be concluded that the gas pressure component is not affected by the selected mesh size (13.3 mm).

From Figure 7, it can be found that a smaller peak reflected pressure for the 1st SW is predicted by the 3D model, which is caused because of the influence of mesh size (as it was discussed in section 2.4). The selected mesh might slightly underestimate the peaks of the reflected shock waves, but it generates similar reflected impulses (Table 2). Therefore, the peak values of the re-reflected SWs could be reduced when a relatively coarse mesh is used that might affect slightly the conclusion about the effectiveness of ventilation associated with mitigation of re-reflected shock waves. The effect of the gas pressure component becomes relatively more important when a coarse mesh is employed, which is conservative for the evaluation of the effectiveness of ventilation to mitigate damage related to the reduction of the gas pressure component.

Several re-reflected SWs with large amplitudes can be observed on the 3D model, which could cause amplification of chamber response due to resonance. For the partially confined condition, SWs decay faster than the fully confined condition.

Table 3 shows the comparison between the peaks reflected pressure and the reflected impulses (including the gas pressure effect) related to the first SW for the fully confined case. In general, the reflected peak pressures ( $p_r$ ) from the 3D model are smaller than those predicted from the UFC approach. It indicates the mesh size effect causes that the peak reflected pressure to be underestimated by 25.6% to 39.3%. In contrast, the reflected impulse related to the 1st SW from the 3D model is higher than that from the simplified UFC model. This is because a secondary reverberating shock wave is modeled by the 3D model. The arrival time related to the 2nd SW ( $t_a^{(2SW)}$ ) is significantly longer than the value that is traditionally assumed by using the simplified approach ( $3t_a$ ), which indicates the second SW propagates slower than the 1st SW, showing that the 2nd SW arrives between  $[3 \cdot t_a - 7 \cdot t_a]$ .

Table 3: The 1<sup>st</sup> SW and the 2<sup>nd</sup> SW arrival time and the peak reflected pressure

$W$ (kg)	$p_r$ (MPa)	$p_r^{UFC}$ (MPa)	$\varepsilon_r$ (%)	$i_r^{(1st SW)}$ (MPa ms)	$i_r^{MSP}$ (MPa ms)	$\varepsilon_r$ (%)	$t_a^{(2SW)}$ (ms)	$3t_a$ (ms)	$t_a^{(2SW)}$ $t_a$
7	7.58	10.19	-25.6	2.01	1.92	4.7	2.413	1.947	3.72
15	12.65	19.70	-35.8	3.96	3.57	11.1	2.247	1.578	4.27
30	20.57	33.79	-39.1	7.05	6.38	10.4	2.106	1.317	4.80
120	52.05	85.79	-39.3	28.55	20.52	39.1	2.196	0.992	6.64



Figure 8 compares the radial displacement from the coupled 3D model and the uncoupled equivalent SDOF system using the pressure time-histories obtained for the fully confined case (3D\_AD-FC) and the partially confined case (3D\_AD-PC) (Figure 7). These results are calculated by using the chamber thickness associated with a ductility ratio of 5 for Case 1S ( $h_{\mu} = 5$  of Table 1). It can be observed that the radial displacement obtained for the fully confined case (3D\_AD-FC-3D) is practically the same at any point in the chamber. In contrast, the radial displacement that was obtained for partially confined chambers (3D\_AD-PC-3D) refers to points far from the opening (indicated as points 1, 2, and 3 in Figure 9). These points show significant differences with other points of the chamber (which are closer to the opening). From Figure 8, it can be observed that the fully confined response of the chamber is governed by the RBM (SDOF system). This is because there are minor differences between the 3D model (3D\_AD-FC-3D) and the SDOF (3D\_AD-FC-SDoF), which is due to a slight time lag between responses, which can be attributed to numerical errors, and small numerical differences between the 3D model and the simplified SDOF model.

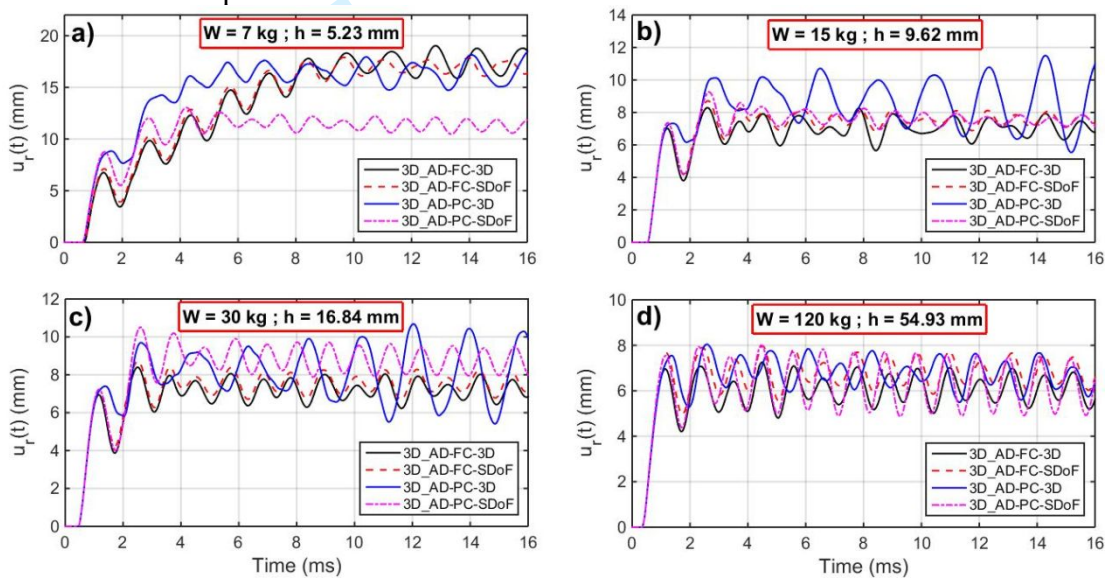


Figure 8 Radial displacement response associated with the pressure time-history obtained for the fully confined (3D\_AD-FC) and partially confined (3D\_AD-PC) cases according to the 3D model and the SDOF model a)  $W=7$ k, b)  $W=15$  kg, c)  $W=30$  kg, d)  $W=120$  kg

16

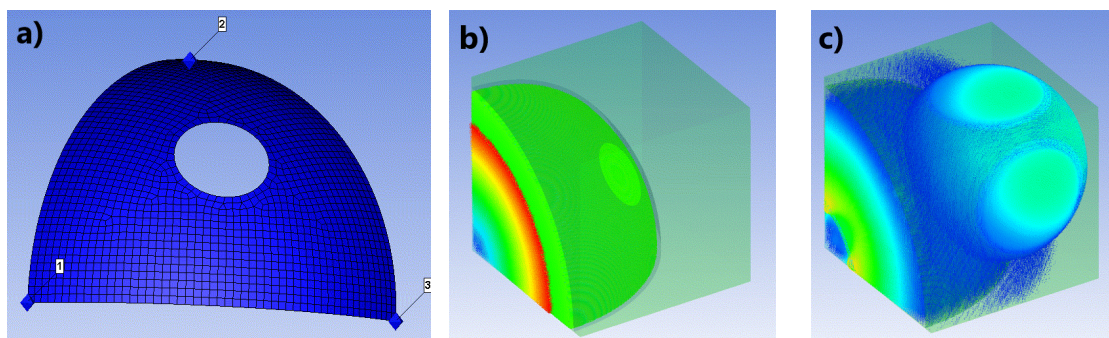


Figure 9 Gauge points far away from openings (related to Figure 8) and gas relief sketch for partially confined chambers; a) mesh and gauges points, b) initial remapping velocities associated with the 1<sup>st</sup> SW, c) relief of gases through openings

Radial displacements obtained for the partially confined case (at points far from openings) are in the same order of magnitude with those obtained from the fully confined case, which indicates that that ventilation is not sufficient to reduce structural responses.

14

1 The chamber response associated with the partially confined cases obtained from the 3D  
 2 model and the equivalent SDOF approach shows significant differences. This is because  
 3 the 3D modeled chamber response is described by several modes rather than only the  
 4 RBM. This can be proved by the response of case 3D\_AD-PC-3D, which is governed by  
 5 lower frequencies than the RBM frequency, indicating that other membranes and  
 6 composite modes are involved in the dynamic response. Results indicate that several re-  
 7 reflected SWs are strong enough to amplify the radial response when TNT weight  
 8  $W=7\text{kg}$ . This result is consistent with the resonance condition that was established in  
 9 Hernandez et al. (2018). That is,  $\Theta = 2 \cdot t_a/T_n + t_0/3 \cdot T_n - t_{max}/T_n + 1/4 \approx 1$  when  
 10  $W=7\text{kg}$  and  $h = h_{\mu=5} = 5.23\text{mm}$ , indicating that SWs tends to coincide with positive  
 11 radial velocities. For  $W=15\text{kg}$  and  $W=30\text{ kg}$ ,  $\Theta \approx 0.77$  and  $\Theta \approx 0.69$ , only the first and  
 12 second SWs are strong enough to amplify the chamber response. For the case that  
 13  $W=120\text{kg}$ , the chamber response was only governed by the 1<sup>st</sup> SW because  $\Theta \approx 0.40$ ,  
 14 which means that secondary re-reflected shock waves coincide with negative velocities  
 15 and do not resonance. It can also be observed that the partially confined chambers show  
 16 higher radial displacements when the response is governed by the 1<sup>st</sup> and the 2<sup>nd</sup> SWs  
 17 (i.e.,  $W=15\text{kg}$ ,  $30\text{kg}$ , and  $120\text{kg}$  in Figure 8). In particular, openings cause that the 2<sup>nd</sup> SW  
 18 generates slightly longer radial amplifications than the observed for the fully confined  
 19 case. On the other hand, the SDOF radial response is mitigated by ventilation when  
 20 several re-reflected SWs are dominant because ventilation is effective in mitigating long-  
 21 term SWs ( $W=7\text{kg}$  in Figure 8). This implies that ventilation might mitigate structure  
 22 response to some instances when resonance due to multiple shock waves occur.

Table 4 Ductility ratio after 1<sup>st</sup> SW (1), 2<sup>nd</sup> SW (2) and final (f)

Case No.	W= 7kg			W= 15 kg			W= 30 kg			W= 120 kg		
	$\mu^{(1)}$	$\mu^{(2)}$	$\mu^{(f)}$	$\mu^{(1)}$	$\mu^{(2)}$	$\mu^{(f)}$	$\mu^{(1)}$	$\mu^{(2)}$	$\mu^{(f)}$	$\mu^{(1)}$	$\mu^{(2)}$	$\mu^{(f)}$
3D_AD-FC-3D	3.5	5.1	9.8	3.6	4.3	4.3	3.6	4.3	4.3	3.6	3.6	3.7
3D_AD-FC-SDoF	3.7	5.3	9.2	3.8	4.5	4.5	3.7	4.5	4.5	3.9	4.1	4.1
3D_AD-FC- $\varepsilon_p$	3.5	5.1	9.4	3.7	4.3	4.3	3.6	4.3	4.3	3.6	3.7	3.8
3D_AD-FC- $\varepsilon_p^{max}$	3.5	5.1	9.4	3.7	4.3	4.3	3.6	4.3	4.3	3.6	3.7	3.8
3D_AD-PC-3D	4.5	7.3	9.5	3.8	5.2	5.9	3.8	5.0	5.5	3.9	4.1	4.1
3D_AD-PC-SDoF	4.5	6.2	6.7	3.8	4.8	4.8	3.7	5.4	5.4	3.9	4.1	4.1
3D_AD-PC- $\varepsilon_p$	3.3	5.1	6.1	2.8	3.4	3.4	2.7	3.2	3.2	2.4	2.4	2.4
3D_AD-PC- $\varepsilon_p^{max}$	3.3	5.2	6.4	2.9	3.5	3.5	2.8	3.3	3.3	2.4	2.4	2.4

23

24 Table 4 shows ductility ratios that are obtained as  $\mu = u_r^{max} / u_{ry}$  (where  $u_r^{max}$  is the  
 25 maximum accumulated radial displacement displayed in Figure 8, and  $u_{ry} = \sigma_y \cdot (1 - \nu)$   
 26  $/ (a \cdot E) = 1.941\text{mm}$  the RBM yielding displacement). For comparison, Table 4 also  
 27 shows ductility ratios that are obtained from the effective plastic strain of the 3D model,  
 28 associated with points that are far from openings (Figure 9), i.e.,  $\mu = \varepsilon_p / (\sqrt{2} \cdot \varepsilon_y) + 1$   
 29 (where  $\varepsilon_p$  = the effective plastic strain computed by the model and  $\varepsilon_y = \sigma_y$   
 30  $/ E = 0.0018$  = the yielding strain). Table 4 summarizes ductility ratios after the 1<sup>st</sup> SW,  
 31 the 2<sup>nd</sup> SW and the final computed value (i.e.,  $t=16\text{ms}$ ). It also shows the ductility ratios  
 32 that are calculated from the maximum plastic strain ( $\varepsilon_p^{max}$ ) associated with top/bottom  
 33 layers of the shell, which includes the effect of bending strains at these positions. It can  
 34 be found that a good agreement is obtained for fully confined chambers in terms of the  
 35 ductility ratio obtained from all derivations, demonstrating that the chamber response is



mainly governed by the RBM. In contrast, the partially confined chamber shows that other membrane modes contribute significantly to the chamber response because results obtained from the 3D model and the SDOF model are significantly different. Similarly, the ductility ratios that are calculated from the plastic strain ( $3D\_AD-PC-\varepsilon_p$  and  $3D\_AD-PC-\varepsilon_p^{\max}$ ) are considerably smaller than values computed from the displacement response obtained from the 3D model or the SDOF approach, which means that the local radial response disagrees with local strain, implying that damage is not uniformly distributed. It can be observed that there are no significant differences of ductility ratios calculated from the effective plastic strain obtained at the mid-plane layer (membrane effect)  $3D\_AD-PC-\varepsilon_p$  and the plastic strain obtained at the top/bottom layer ( $3D\_AD-PC-\varepsilon_p^{\max}$ ), indicating that bending stresses are low, and membrane strains governs the response for points that are far from the openings.

Figure 10 shows the effective plastic strain for the fully confined and partially confined chambers. These are the final effective plastic strain at the middle-plane layer associated with the membrane behavior and at the outer/inner surface layer caused by the combined membrane and bending stresses. These results indicate that both the fully confined and partially confined chambers are governed by membrane strain. The fully confined chambers subjected to concentric spherical TNT detonations have an almost uniform plastic strain distribution, which confirms that the chamber response is described by the RBM. In contrast, the chambers with openings present a variable distribution of its final effective plastic strain, which is concentrated around the opening and along lines that connect these openings. The effective plastic strain that is observed near to the openings is considerably higher than the observed for zones far-off openings, and substantially higher than the values obtained for FC chambers. It can be concluded that openings cause significant geometrical imperfections that trigger the participation of several membrane modes on the chamber response. This asymmetrical membrane response generates stress concentration around openings that produces severe local damage. In contrast, points far-off the opening show slightly lower local damage than fully confined chambers.

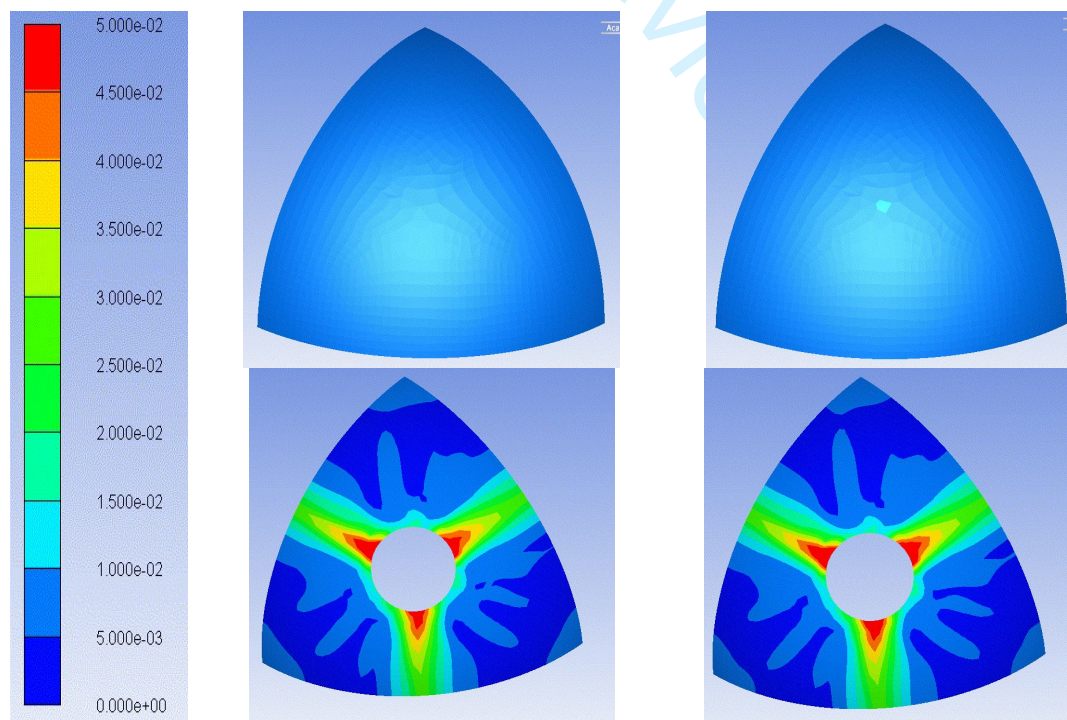


Figure 10 Effective plastic strain ( $\varepsilon_p$ ) related to FC (top) and PC (bottom) chambers ( $a=1500\text{mm}$ ,  $h=9.62\text{mm}$ ,  $W=15\text{kg}$ ) for the middle-plane (membrane strain, on the left) and

surface layer (membrane and bending, on the right)

Figure 11 shows the plastic work that is calculated using the 3D model. It can be observed that at the end of the simulation, there are no significant differences between the partially confined and fully confined chambers, which means the energy absorbed by the chamber (both the global chamber response and damage) does not change significantly for either chamber. Although the overpressure time-history for the partially confined case is mitigated by ventilation, opening leads to weak zones that experience more significant plastic deformations and absorb extra energy. Therefore, chambers with or without openings absorb similar plastic energy. But partially confined chambers are more concentrated and imply more devastating consequences.

In conclusion, numerical modeling using the 3D model indicates that opening is ineffective in mitigating the damage of spherical chambers. Openings weaken the structure and induce local stress and damage concentration during the dynamic response of the chamber. In terms of global chamber response, the radial response of partially confined chambers is almost unaltered by openings, and the total plastic energy of the chamber is similar to the observed for the fully confined chambers. These results confirm the conclusions derived by using the SDOF analysis, which shows that ventilation is ineffective in reducing the chamber response and damage (Hernandez et al., 2018). Moreover, the 3D model shows that damage is not uniformly distributed because of stress concentrations caused by openings, which further enforces the conclusion that small/intermediate openings are not a proper solution to improve the performance of membrane blast chambers.

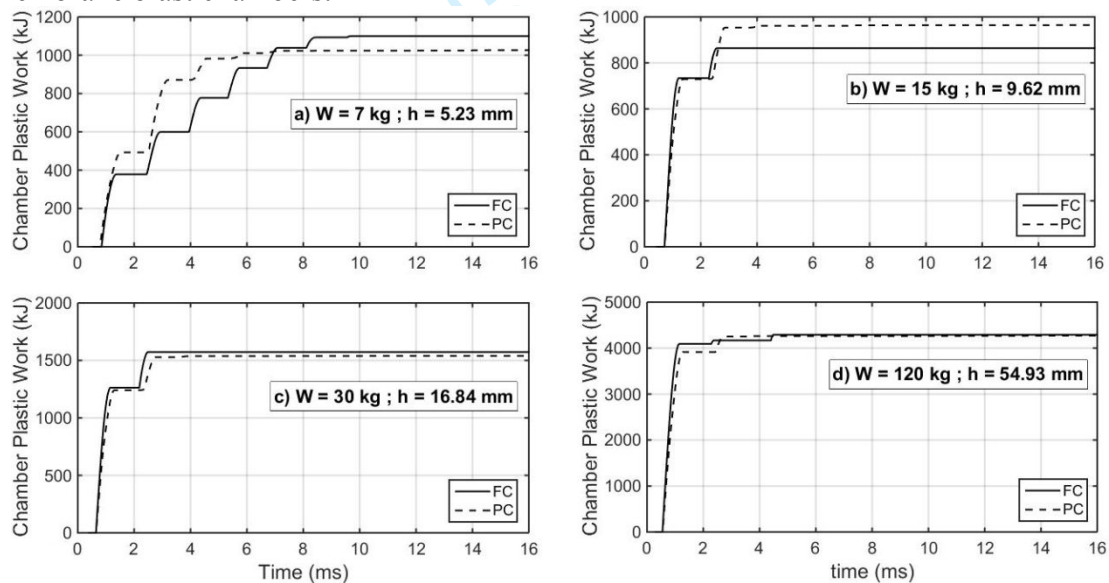


Figure 11 Plastic work for Fully Confined (FC) and Partially Confined (PC) chambers  
a) W=7kg, b) W=15 kg, c) W=30 kg, d) W= 120 kg

## 2.7 Temperature effects

Ventilation reliefs the internal temperature, which is another essential aspect that needs to be taken into account for the design of blast chambers. The enclosed gases increase the internal temperature and pressure because the HE chemical energy (released during the detonation and the afterburning) is transferred to gases increasing their internal and kinetic energy. The kinetic energy refers to SWs, and the internal energy is associated with the gas pressure component. At a later stage, the confined gas inside the fully confined chambers reaches a constant temperature and pressure associated with the quasi-



static state. In contrast, the internal temperature is rapidly reduced throughout openings, which allows the faster release of gases, and the temperature is rapidly reduced until it reaches the outside temperature. Therefore, the QS temperature is avoided if ventilation is provided, but a high flash internal temperature is observed. After the dynamic response of the chamber, a significant final temperature is observed for the fully confined chambers associated with the QS state. For example, the chemical equilibrium predicts that the final temperature of the gas mixture is approximately equal to  $T_{QS} = 2800\text{K}$  when chambers are deficient in oxygen, i.e.,  $W/V_{\text{vessel}} > 0.387\text{kg-TNT/m}^3$  (Edri et al., 2013). This temperature is so high that ventilation seems to be mandatory, taking into account that the forging temperature for carbon steels is approximately 1500K.

Figure 12 shows the temperature time-history obtained from the 3D model associated with the fully confined and partially confined chambers. It can be observed that openings allow the faster reduction of temperature (in the scale of milliseconds). The fully confined cases show significant QS temperatures (i.e., 1900K, 2600K, 3500K, and 6900K for  $W=7\text{kg}$ , 15kg, 30kg, and 120kg, respectively). All the studied cases refer to deficient in oxygen chambers (i.e.,  $W/V_{\text{vessel}} > 0.387\text{ kg TNT/m}^3$ , Table 1) and should show a final QS temperature of 2800K in agreement with the chemical equilibrium (Edri et al., 2013). Nevertheless, it can be observed that the QS temperature that is calculated from the 3D model disagrees with those from the chemical equilibrium approach because gases are modeled by independent EOS and are not described such as a unique gas that should be modeled by a variable gamma ideal gas EOS (Edri et al., 2013; Hernandez et al., 2016).

Ventilation reduces the exposition time that chambers are subjected to high temperatures, generating a flash temperature, and avoiding that the final QS temperature is reached. This aspect should be considered in the design of explosion chambers, and may make mandatory to provide ventilation when the blast load density is relatively high (e.g.,  $W/V_{\text{vessel}} > 0.03\text{ kg-TNT/m}^3$  related to  $T_{QS} = 650\text{K}$  (Edri et al., 2013)). This second design aspect needs to be further studied, considering proper material models that account for temperature effects, and by using approaches that allow predicting the dynamics of the internal temperature that AUTODYN is unable to model reliably.

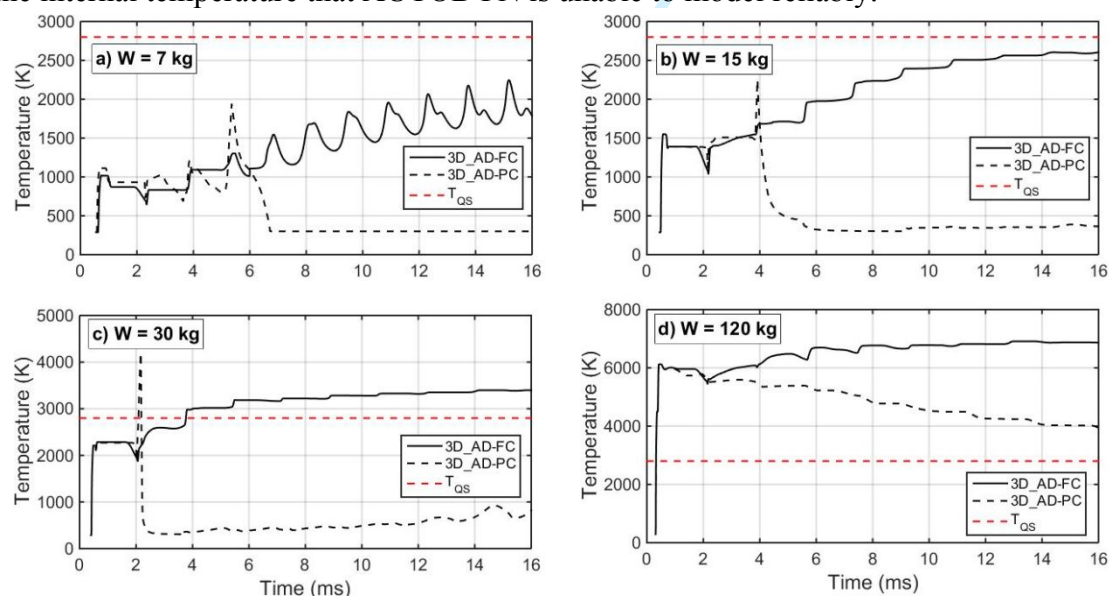


Figure 12 Temperature time histories for the Fully Confined (FC) and Partially Confined (PC) chambers a)  $W=7\text{kg}$ , b)  $W=15\text{ kg}$ , c)  $W=30\text{ kg}$ , d)  $W=120\text{ kg}$

18

### 3 Spherical Chambers subjected to eccentric TNT detonations

When a monobloc spherical chamber is subjected to a concentric spherical HE detonation, the blast overpressure can be described by a uniform blast loading acting on the chamber walls. Therefore, the chamber response is only described by the RBM because the modal force is null for another mode in agreement with the mode orthogonality law. When the chamber or the blast loading does not satisfy a perfect spherical symmetry, other membrane and composite modes will contribute to the chamber response. Previous studies on strain growth of the spherical chamber response showed that structural perturbation such as nozzles or flanges could introduce localized deformations (Abakumov et al., 1984; Karpp et al., 1983), which is confirmed from the 3D model of partially confined chambers. Previous numerical model related to uniform initial impulses shows strain growth due to linear and nonlinear modal coupling response, indicating small imperfections (associated with imperfect spherical geometry) can induce the contribution of composite modes after multiple cycles of vibration (Dong et al., 2010). In the meanwhile, the 3D model showed a stable RBM response, which is attributed to the accuracy of the AUTODYN solution, and the gas pressure component avoided an unstable RBM response. Imperfections of the spherical response occur by different reasons such as heterogenic imperfections of the material, geometrical perturbations, and asymmetries of the blast loading. In particular, the blast loading can be affected by internal asymmetries of the charge, such as an incorrect shape of the charge, its incorrect position, or its incorrect detonation point. In agreement with Sostegard's assumption (McIvor, 1966), the response of spherical chambers can be affected by slight impulse imperfections. To examine the influence of unsymmetrical detonation, the spherical TNT charge is placed 150mm from the center of the spherical chamber ( $a=1500\text{mm}$ ,  $h=9.62\text{mm}$ ,  $W=15\text{kg}$ ). This eccentricity is equivalent to 10% of the main radius. The results of the simulation show that the peak reflected pressure is increased from 19.5MPa to 25.1MPa, and generates nonuniform pressure profiles.

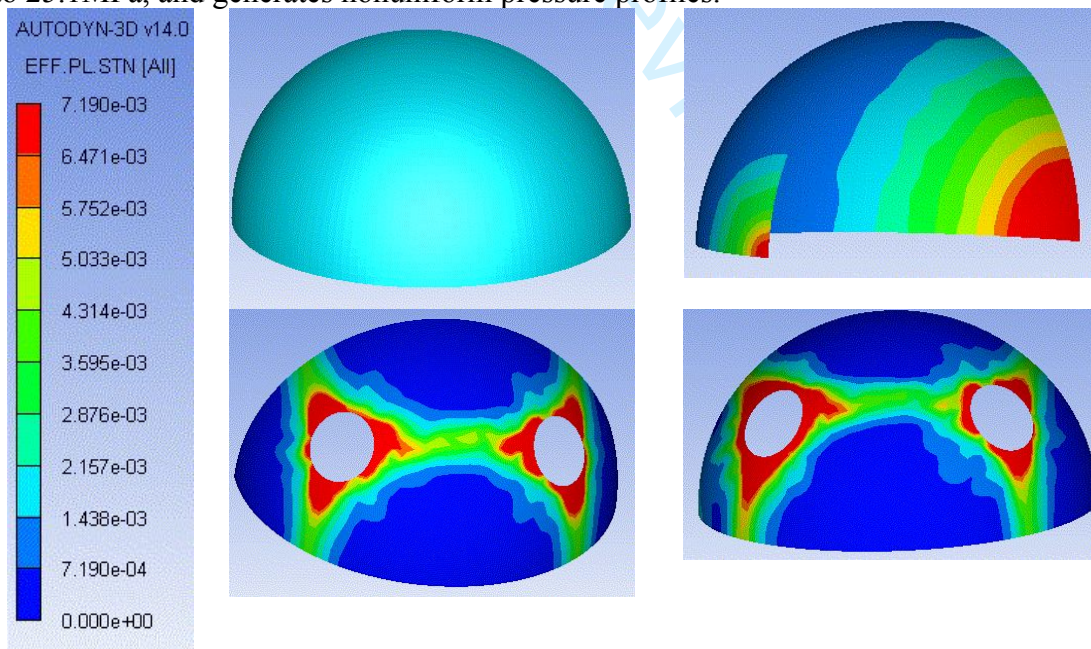


Figure 13 Effective plastic strain ( $\epsilon_p$ ) of the FC (top) and PC (bottom) chambers ( $a=1500\text{mm}$ ,  $h=9.62\text{mm}$ ,  $W=15\text{kg}$ ) for the middle-plane (membrane) with concentric (left) and eccentric TNT charges (right)

28 Figure 13 shows the membrane effective plastic strain of the fully confined (top) and

1 the partially confined chambers (bottom) corresponding to concentric TNT charges (left)  
2 and eccentric TNT charges (right). It can be observed that eccentric detonations generate  
3 localized damage near and opposite to the place where the charge was located, indicating  
4 that eccentric charges induce the response of other modes besides the RBM. It can also  
5 be observed that eccentric explosions also generate significant damage around openings.  
6 Therefore, it can be concluded that opening is not necessarily a proper choice to reduce  
7 damage, although it relieves blast loads and high temperatures associated with confined  
8 detonations. Results of these simulations demonstrate that imperfections such as  
9 eccentricity TNT charge weights can generate significant localized damage, and should  
10 be studied with FEA. Therefore, the correct design of explosion chambers should  
11 consider possible perturbations associated with the blast loading and geometrical  
12 imperfections because such imperfection can generate more considerable localized  
13 damage.

#### 14 **4 Conclusions**

15 This paper carried out numerical simulations on fully and partially confined spherical  
16 chambers subjected to internal detonations. Overall, openings modify the pressure time-  
17 history by reducing the gas pressure component and also mitigates secondary re-reflected  
18 shock waves. The structural response of a spherical chamber subjected to a concentric  
19 detonation is described by the radial breathing mode and can be simplified by an SDOF  
20 system. It was observed that the natural frequencies of spherical chambers could be  
21 significantly high and comparable with the reverberation frequency that the SWs  
22 impinges the chamber wall. In this context, shock waves play the leading role in the  
23 dynamic response. Despite that the pressure component can also play a significant role  
24 on the chamber response, its reduction due to small/intermediate ventilation can be  
25 ignored as the peak dynamic response is not significantly reduced due to ventilation,  
26 because the peak response is observed during the initial phase of the response (due to the  
27 effect of the initial shock waves and when the gas pressure component is not significantly  
28 mitigated). Moreover, it has been observed that the secondary re-reflected shock waves  
29 can amplify the structural response due to elastic or plastic resonance. In contrast, the  
30 presence of opening can modify the structural response generating local weaknesses that  
31 can produce local damage due to stress concentration.

32  
33 The numerical results were compared and found to agree well with the authors' simplified  
34 SDOF. Through numerical simulation, it was found that small/intermediate openings are  
35 ineffective in mitigating the damage of membrane chambers during the vibratory  
36 response phase. Openings can generate stress concentrations and localized damages,  
37 which can reduce the capacity of the blast chamber to resist internal detonations.  
38 Nevertheless, ventilation allows relieving the QS temperature that is observed when fully  
39 confined explosions occur, which can make mandatory to use ventilation when the blast  
40 density is high (e.g.,  $W/V_{vessel} > 0.03 \text{ kg-TNT/m}^3$ ).

41 Coupled and uncoupled 3D models demonstrate that the RBM governs the responses  
42 of FC spherical chambers subjected to concentric HE detonation. So the equivalent SDOF  
43 analysis is accurate to model the chamber response when perfect spherical symmetry is  
44 analyzed. Strong shock waves could force the chamber to respond plastically and  
45 resonate with the re-reflected shock waves, which can increase the chamber response  
46 significantly.

47 The current simplified approach that is used to model re-reflected shock waves might  
48 lead to significant underestimation/overestimation of chamber responses owing to the  
49 inaccurate assumption of the propagation velocity associated with secondary shock waves



20

and its attenuation. Geometrical chamber and blast singularities should be considered for the design of blast chambers because they can drastically modify the chamber performance generating localized damage and variations of the chamber response. Therefore, 3D FEA should be used to model the blast loading, accurately and chamber imperfections that simplified approaches are unable to model.

Ventilation seems to be ineffective in mitigating the damage of membrane vessels, owing to the reduction of the gas pressure component is not fast enough to reduce significantly the maximum response and damage of structures, whose response is described by high frequencies. In the meanwhile, membrane chambers are susceptible to resonance due to re-reflected shock waves. Despite that ventilation mitigates re-reflected shock waves, its effect seems to be smaller than the negative effect generated by the local damages induced by openings. In contrast, structures that respond slowly, such as cubical chambers, display an initial bending response associated with lower frequencies; therefore, they can be significantly affected by the reduction of the gas pressure component and ventilation. Therefore, ventilation could be useful if chambers are governed by initial low frequencies, owing to that the peak response is related to the impulse observed until the peak response is observed.

## ACKNOWLEDGMENTS

The authors acknowledge partial financial supports from the Australian Research Council (ARC) carrying out this research. The first author acknowledges the Chilean government for providing scholarship to study a Ph.D. program in Australia. The authors also acknowledge the support from China National 973 project [2015CB058003] for carrying out field blasting tests for this project.

## REFERENCES

- Abakumov, A.I., Egunov, V.V., Ivanov, A.G., Uchaev, A.A., Tsypkin, V.I., Shitov, A.T., 1984. Calculation and experiments on the deformation of explosion-chamber shells. *J. Appl. Mech. Tech. Phys.* 25, 455–458. <https://doi.org/10.1007/BF00910411>
- Adishchev, V.V., Kornev, V.M., 1979. Calculation of the shells of explosion chambers. *Combust. Explos. Shock Waves* 15, 780–784. <https://doi.org/10.1007/BF00739869>
- Anderson, C.E., Baker, W.E., Wauters, D.K., Morris, B.L., 1983. Quasi-static pressure, duration, and impulse for explosions (e.g. HE) in structures. *Int. J. Mech. Sci.* 25, 455–464. [https://doi.org/10.1016/0020-7403\(83\)90059-0](https://doi.org/10.1016/0020-7403(83)90059-0)
- Baker, W.E., Allen, F.J., 1958. The response of elastic spherical shells to spherically symmetric internal blast loading, in: *Third U.S. National Congress of Applied Mechanics*, ASME, New York. pp. 79–87.
- Belov, A.I., Belyaev, V.M., Kornilo, V.A., Marchenko, A.I., Romanov, G.S., Chernukha, V.V., 1986. Calculation of wall loading dynamics in a spherical combustion chamber. *Combust. Explos. Shock Waves* 21, 132–135. <https://doi.org/10.1007/BF01463688>
- Buzukov, A.A., 1980. Forces produced by an explosion in an air-filled explosion chamber. *Combust. Explos. Shock Waves* 16, 555–559. <https://doi.org/10.1007/BF007949334.004>



- 1  
2  
3 1 Dong, Q., Hu, B.Y., Chen, S.Y., Gu, Y., 2012. Engineering Design of a Multiple-Use  
4 2 Spherical Explosion Containment Vessel Subjected to Internal Blast Loading From  
5 3 25 kg TNT High Explosive. *J. of Press. Vessel Technol.* 134, 1–5.  
6 4 <https://doi.org/10.1115/1.4005397>  
7  
8  
9 5 Dong, Q., Li, Q.M., Zheng, J.Y., 2010. Further study on strain growth in spherical  
10 6 containment vessels subjected to internal blast loading. *Int. J. Impact Eng.* 37,  
11 7 196–206. <https://doi.org/10.1016/j.ijimpeng.2009.09.001>  
12  
13 8 Dong, Q., Li, Q.M., Zheng, J.Y., 2011. Guidelines for the Design of Multiple-Use  
14 9 Explosion Containment Vessels Based on the Understanding of the Strain Growth  
15 10 Phenomenon. *J. Constr. Facil.* 25, 394–400.  
16 11 [https://doi.org/10.1061/\(ASCE\)CF.1943-5509.0000182](https://doi.org/10.1061/(ASCE)CF.1943-5509.0000182).  
17  
18  
19 12 Duffey, T.A., Romero, C., 2003. Strain growth in spherical explosive chambers  
20 13 subjected to internal blast loading. *Int. J. Impact Eng.* 28, 967–983.  
21 14 [https://doi.org/10.1016/S0734-743X\(02\)00169-0](https://doi.org/10.1016/S0734-743X(02)00169-0)  
22  
23  
24 15 Edri, I., Feldgun, V.R., Karinski, Y.S., Yankelevsky, D.Z., 2012. On blast pressure  
25 16 analysis due to a partially confined explosion: III. afterburning effect. *Int. J. Prot.*  
26 17 *Struct.* 3, 311–331. <https://doi.org/10.1260/2041-4196.3.3.311>  
27  
28  
29 18 Edri, I., Feldgun, V.R., Karinski, Y.S., Yankelevsky, D.Z., 2013. Afterburning aspects  
30 19 in an internal TNT explosion. *Int. J. Prot. Struct.* 4, 97–116.  
31 20 <https://doi.org/10.1260/2041-4196.4.1.97>  
32  
33  
34 21 Hernandez, F., 2016. Explosive Protection of Storage Chambers through Frangible  
35 22 Structural Elements. The University of Western Australia.  
36  
37 23 Hernandez, F., Hao, H., Abdel-Jawad, M., 2016. Additional afterburning energy value  
38 24 to simulate fully confined trinitrotoluene explosions. *Int. J. Prot. Struct.* 7, 232–  
39 25 264. <https://doi.org/10.1177/2041419616640113>  
40  
41 26 Hernandez, F., Hao, H., Zhang, X., 2018. On the effectiveness of ventilation to mitigate  
42 27 damage of spherical chambers subjected to confined trinitrotoluene detonations.  
43 28 *Adv. Struct. Eng.* 1–16. <https://doi.org/10.1177/1369433218791610>  
44  
45  
46 29 Karpp, R.R., Duffey, T.A., Neal, T.R., 1983. Response of Containment Vessels to  
47 30 Explosive Blast Loading. *J. Press. Vessel Technol. Trans. ASME* 105, 23–27.  
48 31 <https://doi.org/10.1115/1.3264234>  
49  
50  
51 32 Li, Q.M., Dong, Q., Zheng, J.Y., 2008. Strain growth of the in-plane response in an  
52 33 elastic cylindrical shell. *Int. J. Impact Eng.* 35, 1130–1153.  
53 34 <https://doi.org/10.1016/j.ijimpeng.2008.01.007>  
54  
55 35 McIvor, I.K., 1966. Axisymmetric Response of a Closed Spherical Shell to a Nearly  
56 36 Uniform Radial Impulse. *J. Acoust. Soc. Am.* 40, 1540.  
57 37 <https://doi.org/10.1121/1.1910260>  
58  
59  
60 38 Moss, D., 2004. *Pressure Vessel Design Manual*, 3rd ed. Gulf Professional Publishing.

1  
2  
3  
4  
5  
6  
7  
8  
9  
10  
11  
12  
13  
14  
15  
16  
17  
18  
19  
20  
21  
22  
23  
24  
25  
26  
27  
28  
29  
30  
31  
32  
33  
34  
35  
36  
37  
38  
39  
40  
41  
42  
43  
44  
45  
46  
47  
48  
49  
50  
51  
52  
53  
54  
55  
56  
57  
58  
59  
60

22

1 Shin, J., Whittaker, A.S., Cormie, D., Wilkinson, W., 2014. Numerical modeling of  
2 close-in detonations of high explosives. *Eng. Struct.* 81, 88–97.  
3 <https://doi.org/10.1016/j.engstruct.2014.09.022>

4 Trabia, M.B., O'Toole, B.J., Thota, J., Matta, K.K., 2008. Finite Element Modeling of a  
5 Lightweight Composite Blast Containment Vessel. *J. Press. Vessel Technol.* 130,  
6 011205 1–7. <https://doi.org/10.1115/1.2826437>

7 UFC 3-340-02, 2008. Structures to Resist the Effects of Accidental Explosions,  
8 Structures Congress 2011. Unified Facilities Criteria - Department of Defense  
9 USA. [https://doi.org/10.1061/41171\(401\)127](https://doi.org/10.1061/41171(401)127)

10 Zhdan, S.A., 1981. Dynamic Load Acting on the Wall of an Explosion Chamber.  
11 *Combust. Explos. Shock Waves* 17, 241–244. <https://doi.org/10.1007/BF00770841>

12

For Peer Review